Study of Grafting Propylene–Ethylene Block Copolymer

HSIEN-TANG CHIU, WEI-MING CHIU

Graduate School of Textile and Polymer Engineering, National Taiwan Institute of Technology, Taipei, Taiwan

Received 28 April 1997; accepted 27 October 1997

ABSTRACT: The article describes the mechanical properties of a propylene–ethylene block copolymer (Co-PP) used as a matrix with acrylic acid (AA) and strengthened with glass fiber. Isotactic polypropylene (i-PP) is also used as a matrix to compare with the results obtained from the Co-PP grafting. Experimental results indicate that AA grafting improves the interfacial adhesion between the matrices and glass fiber. AA grafting also enhances the mechanical properties of glass fiber-reinforced polypropylene (FRPP). A quantitative titration is performed to analyze the grafting ratio and grafting efficiency. In addition, the specimens are injection-molded to investigate the mechanical properties and morphologies. In addition, the effects on the matrix structure, attributed to the grafting and blending of the glass fiber, are also investigated. © 1998 John Wiley & Sons, Inc. J Appl Polym Sci 68: 977–988, 1998

Key words: grafting; melt-mixing; propylene–ethylene block copolymer; polypropylene; glass fiber

INTRODUCTION

It is highly desirable for a plastic matrix, with a functional group reaction within itself, to form a chemical bond with a functional group of treated fillers. If able to do so, the reinforced composite material has more significant performance properties than has the initial matrix. While adopting this notion, Sasaki and many other investigators employed the graft-copolymerization method[1–5] to graft copolymerize monomers—unsaturated carboxylic acid, anhydride, and acrylate—on polypropylene to improve the adhesion of polypropylene and, ultimately, the adhesion between various filler interfaces. Among the above-mentioned monomers, grafting unsaturated carboxylic acid leads to the greatest improvement after modification. Furthermore, interfacial adhesion between fillers and the plastic matrix significantly increase the performance of the composite materials, thereby necessitating the need to improve the interfacial adhesion of the reinforcing material. As for mineral fillers, multiple coupling agents are also used in the surface finish, such as in the treated surface functional group.[6–11] Polarized monomer is also grafted onto the glass fiber surface by using ionic polymerization.[12–16] All methods are employed to increase the adhesion of the filler's surface, wet the surface of the plastic matrix better, and, finally, improve the interfacial adhesion between the plastic matrix and the glass fiber. Three graft-copolymerization methods are conventionally used for grafting carboxylic acid monomer on polyolefines: the radiation method, solution reaction method, and melt-mixing method. Among those, the melt-mixing method is considered the most simple, economical, efficient, and appropriate for industrial purposes.

Although isotactic polypropylene (i-PP) has been extensively studied in grafting research,[1–16] the polypropylene copolymers (Co-PP) have seldom been mentioned. Co-PP has the following merits: (1) Co-PP is a block copolymer, retaining a high crystallinity. Restated, Co-PP retains good stiffness qualities as well as service temperature and other characteristics of i-PP; and (2) Co-PP displays a better impact strength than that of i-PP, particularly the low-temperature impact

Correspondence to: H.-T. Chiu.

Journal of Applied Polymer Science, Vol. 68, 977–988(1998)
 CCC 0021-8995/98/060977-12

strength, due to the lower glass transition temperature (T_g) of the ethylene–propylene interface of Co-PP. In this work, we applied the grafting method of melt-mixing the monomer acrylic acid (AA) to the propylene–ethylene block copolymer (Co-PP) using benzoyl peroxide (BPO) as an initiator. Meanwhile, i-PP is used as a control matrix to compare the results of the Co-PP grafting research. The glass fiber is treated with coupling agents—aminosilane or epoxysilane. More specifically, in the general formula —(RO)3SiR′X, X is substituted for —NH2 and 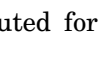 . These two functional groups not only form a chemical bond with —COOH of PP-*g*-AA in the high-temperature blending process, but also facilitate adhesion between the interfaces of the glass fiber and PP. The PP is usually formed into a complex structure by adding mineral fillers for reinforcing purposes. Overall, most fillers contribute to reinforcing the matrix mechanical properties; in most cases, fibrous fillers yield the optimum results. Therefore, glass fiber is selected herein as the reinforcing material. In addition, the effects on the interface of composite materials from grafting matrices and fillers in a twin-screw extruder are also studied.

EXPERIMENTAL

Materials

The matrices used herein included the propylene–ethylene block copolymer (Co-PP) from Aristech Chemical Co (USA), product no. IT-4070-GPP-3080, with a melt flow index (MFI) of 7.6 g/min, and i-PP supplied by Yuan Chia Chemical Industries Co. (Taiwan), product no. Yuan Chia PP-1080, with an MFI of 8.0 g/min. The two kinds of glass fiber used as reinforcing material (manufactured by Min Da Industries Co. (Taiwan)) were (a) a short fiber of L = 6 mm and D = 13 μm, treated with a coupling agent of aminosilane [Union Carbide A-1100 $H_2NC_3H_6Si(OCH_2CH_3)_3$] and (b) a short fiber of L = 6 mm and 13 μm, treated with a coupling agent of epoxysilane [Union Carbide A-187, $CH_3CH_2CH_2OC_3H_6Si(OCH)_3$]. Lin-Chwen-Yuh (Taiwan), an AA monomer, was used in the grafting process. The initiator used was benzoyl peroxide (BPO), a product for experimental purposes manufactured by Chia Hwa Chemical (Taiwan). Xylene, methanol, potassium hydroxide (KOH), and acetone all served as Lin-Chwen-Yuh (Taiwan), a level 1 product for experimental purposes.

Preparation for Reinforcement Matrices

Melt-Grafting Matrices

First of all, the monomer AA and the initiator BPO were dissolved and stirred until completely dissolved in acetone. The solution was then fully mixed with matrix powder (below 50 μm mesh), as prepared at a low temperature. Later, the mixture was exposed to air, allowing the acetone to evaporate completely. The final mixture was grafted in a twin-screw extruder, using the melt-mixing method. The setting temperatures for various stages of the extruding screw were 140, 180, 200, and 210°C, and the speed of the extruding screw was 25 rpm.

Quantitative Analysis of Grafting Ratio and Grafting Efficiency

About 8.0 g of matrix powder was poured into a flask dipped with 300 mL xylene/methanol in a 2 : 1 mixed solution and boiled and refluxed for 8 h. The extracted solution was titrated with a 0.05*N* KOH/methanol solution to obtain the weight (W_1) of the grafted AA (M-*g*-AA) and poly(acrylic acid) (PAA). About 2.0 g of M-*g*-AA powder was dissolved in 100 mL of the xylene solution before 100 mL of distilled water was added for extraction. The water layer, obtained using a separator funnel, was titrated with a 0.05*N* KOH/methanol solution to obtain the weight (W_2) of PAA. The grafting ratio and grafting efficiency could thus be obtained by the following two equations[7,17,18]:

$$\text{Grafting ratio (\%)} = \frac{W_1 - W_2}{\text{wt of original sample}} \times 100\% \quad (1)$$

$$\text{Grafting efficiency} = \frac{W_1 - W_2}{W_1} \times 100\% \quad (2)$$

Preparations for FRPP and FRPP Blends

The AA grafting matrix materials and glass fiber were initially dried and mixed in various ratios. After melt-mixing the mixture in a twin-screw extruder, the mixture was cut into a chip. The chips were then dried in a vacuum oven with the temperature set at 80°C for 2 days and, finally, made into various specimens to comply with the ASTM standard for injection molding, using a Toshiba

Is-55 EPN injection-mold model, under the following parameters: temperature set at 220, 230, 240, and 230°C for various stages of extruding, injection pressure at 1000 psi, and mold temperature set at 60°C. Herein, the matrices, Co-PP and i-PP, also underwent the above processes for blank tests to obtain the same thermal and processing histories.

Test Methods

The specimen was scanned for observation using a scanning electron microscope: Cambridge S : 360. Initially, it was coated with gold using an Ion sputter at 10 mA for 4 min and, then, photographed using a 55 Polaroid to investigate its structure. For Fourier transfer infrared (FTIR), an FT/IR-3 of the Japan Spectroscopic Co. was utilized. The specimens were made by heat compressing the material at 190°C into a film of approximately 25 μm thick. Next, Izod impact testing was conducted using Amityville TMI No. 43-1 equipment, according to the ASTM D-256 test method. A temperature chamber adapted to the Izod impact testing machine was then used to provide a constant chamber temperature. The chamber was equipped with a resistance coil (heat), a liquid nitrogen coolant, an internal fan, and a digital thermometer. The sample was held in the chamber at the testing temperature for more than 30 min before it was tested. Next, the tensile strength was tested using a Hung Ta-8503 tester according to the following method: ASTM-D638-Type I with a drawing speed of 10 mm/min and a span length of 25 mm. The flexural strength and modulus testing method, ASTM-D790-method-II procedure B, used 4-point loading at 1/4 points with a crosshead speed of 1.8 mm/min, span length of 25 mm, and load of 40 kgw, at 65% RH and room temperature. The heat-distortion temperature (HDT) test was then conducted according to ASTM D648, using Ceast 6510 equipment, with a 445 kPa stress and a temperature increase rate of 2°C/min. In addition, a wide-angle X-ray diffractometer (WAXS) of Shimadzu X-ray was used. Finally, a diffractomter XD-5 was used with CuKα radiation, scanning angle of 2θ (from 5° to 30°), scanning rate of 4/min, and an injecting-molded specimen sized $3 \times 13 \times 20$ mm.

RESULTS AND DISCUSSION

Analysis of Grafting Ratio and Grafting Efficiency for AA

Figure 1(a) depicts the SEM photos of Co-PP-*g*-AA (5 phr AA), both of which were washed away with PAA by xylene, while (b) is an SEM photo of the PAA and AA side chain which was washed away by xylene/MeOH (2/1) extraction for 8 h. Figure 1(b) clearly indicates that particles entirely disappeared in Co-PP-*g*-AA (5 phr) after going through xylene/MeOH (2/1) extraction for 8 h. Restated, the AA side chains were completely extracted, thereby confirming the accuracy of our subsequent qualitative and quantitative analyses.

With the functional group C═O of AA, a strong absorption peak appears at wavenumber 1720 cm^{-1} using FTIR which is not observed in the PP structure. Therefore, by using FTIR, AA grafting on Co-PP is quickly analyzed. Figure 2 displays the differences in FTIR figures between Co-PP prior to and after AA grafting with AA concentrations of 1, 3, 5, and 7 phr. Prior to the FTIR test, PAA was also extracted from all Co-PP-*g*-AA samples using xylene. Therefore, the magnitude of amplitude for the absorption peak at 1720 cm^{-1} in FTIR represents the quantity of AA grafted on PP. From the results in Figure 2, we can infer that the grafting quantity on Co-PP increases with an increasing AA concentration.

Figure 3 illustrates the variations in the grafting ratios of Co-PP and i-PP with the BPO initiator fixed at 1 phr and AA concentrations of 1, 3, 5, and 7 phr. This figure clearly indicates that the grafting ratio of Co-PP and i-PP increases with an increasing AA concentration; however, the grafting ratio of i-PP surpasses that of Co-PP, which may be attributed to that a 3^0H on the i-PP molecular structure is more than that of Co-PP. A further explanation is that the hydrogen atom of alkanes tend to be abstracted as follows: $3^0H > 2^0H > 1^0H > CH_4$. Restated, 3^0H is most easily abstracted to form a free radical, accounting for why the grafting ratio of i-PP always surpasses that of Co-PP. Figure 4 depicts variations of the grafting efficiency of Co-PP and i-PP with the BPO initiator fixed at 1 phr and the AA concentration at 1, 3, 5, and 7 phr. According to this figure, the grafting efficiencies of both Co-PP and i-PP decrease with an increasing AA concentration. Such a phenomenon can be attributed to the defining equation of grafting efficiency (%) = $[(W_1 - W_2)/W_1] \times 100\%$: As AA concentration increases, the quantity of PAA (W_2) also increases and the grafting efficiency is subsequently decreased.

Study of Mechanical Properties of Grafting Matices

Notched Izod Impact Strength

Figure 5 displays the variations of the notched Izod impact strength of Co-PP and fiber-rein-

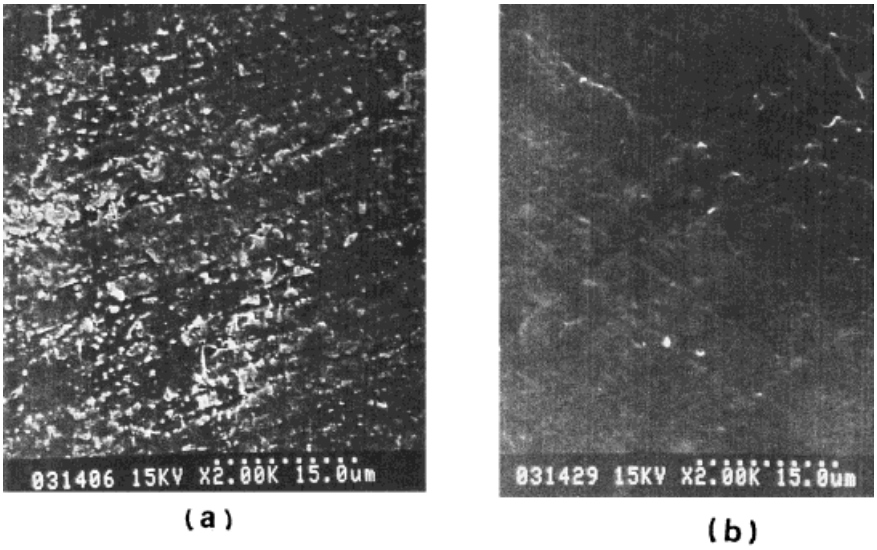

Figure 1 Scanning electron micrographs of (a) Co-PP-*g*-AA (5 phr AA, unextracted) and (b) Co-PP-*g*-AA (5 phr AA, extracted with xylene/MeOH solution) film.

forced PP (FRPP) at various temperatures. As this figure reveals, the notched Izod impact strength of Co-PP is sensitive toward the temperature change. For instance, the notched impact strength decreases when the temperature falls below 0°C. Figure 6 depicts the variations for the i-PP FRPP system. According to this figure, the Izod impact strength of i-PP is more sensitive to the temperature change. When the temperature is lower than 0°C, the notched impact strength

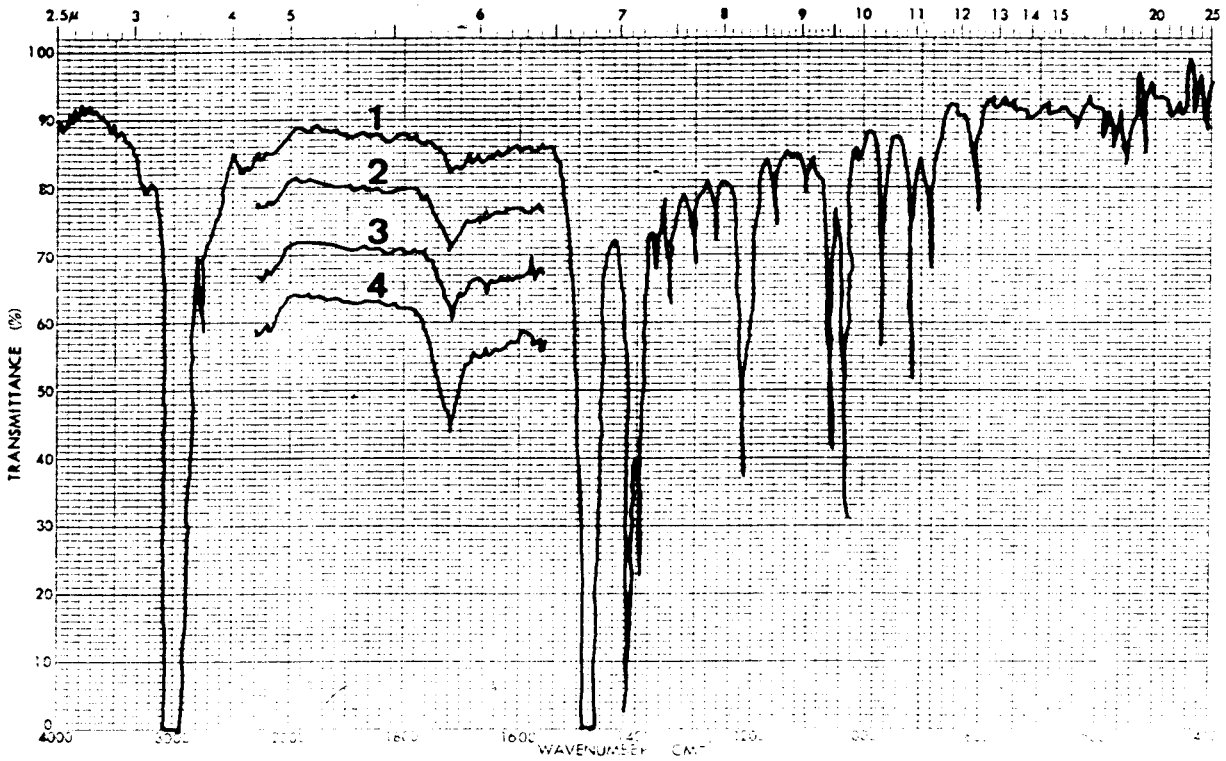

Figure 2 FTIR spectra of Co-PP grafted with AA, sample recovered after extraction with xylene: (1) Co-PP grafted with 1 phr AA; (2) Co-PP grafted with 3 phr AA; (3) Co-PP grafted with 5 phr AA; (4) Co-PP grafted with 7 phr AA.

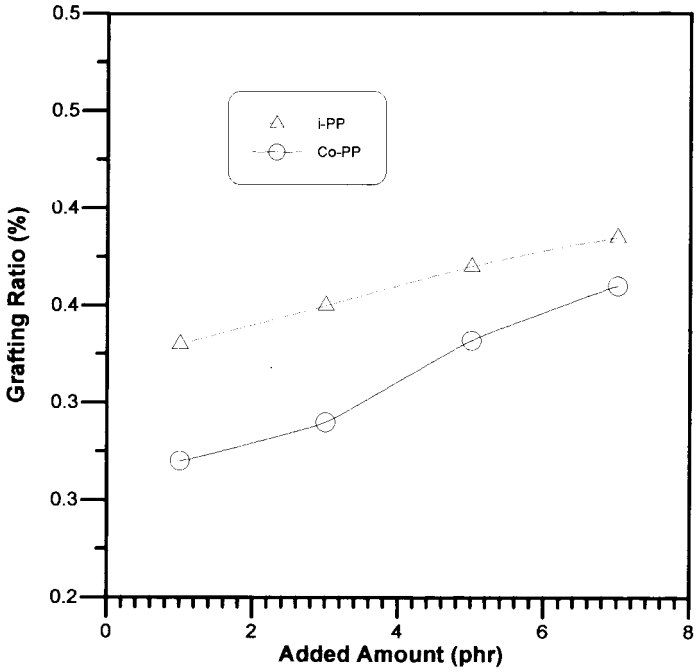

Figure 3 Effect of AA on grafting ratio.

markedly decreases, demonstrating the brittleness of i-PP. After the blends undergo glass-fiber reinforcement, its notched Izod impact strength remains constant, independent of the temperature. This phenomenon is attributed to that glass fiber effectively absorbs the impact energy. Experimental results also confirm the reinforcing effect on the epoxysilane-treated glass fiber (EGF) is

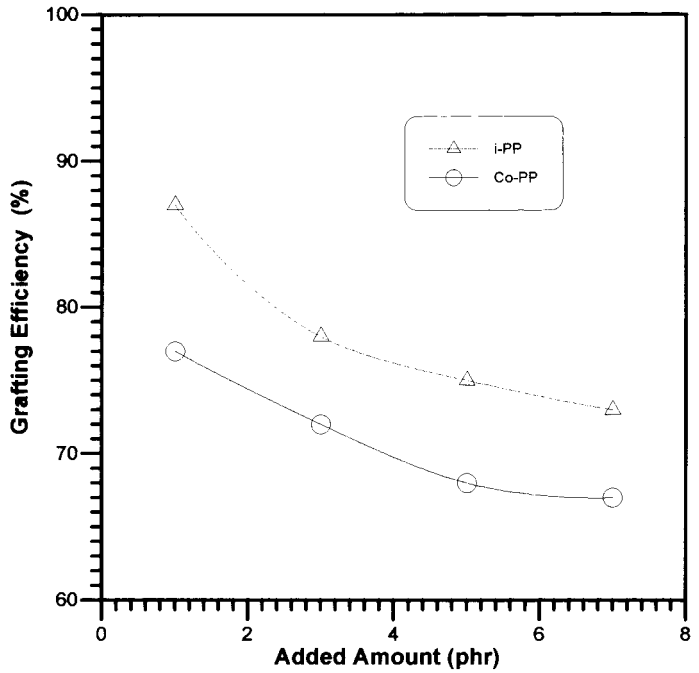

Figure 4 Effect of AA on grafting efficiency.

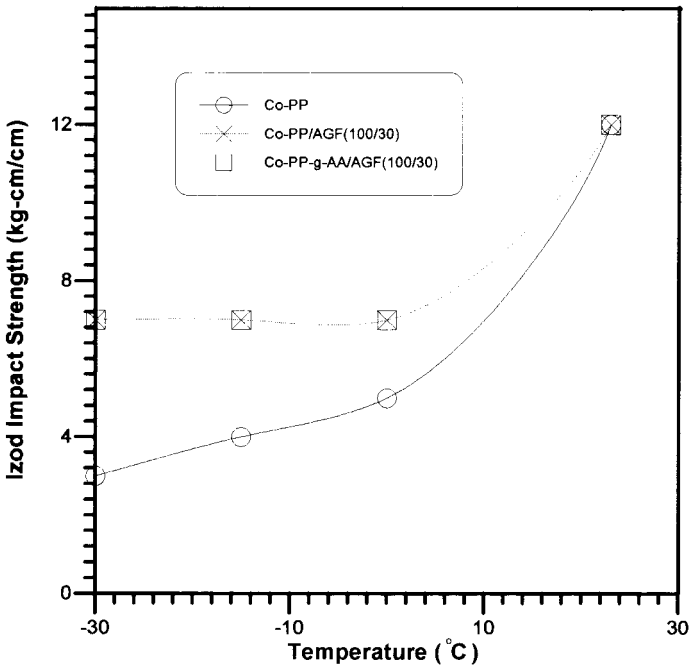

Figure 5 The notched Izod impact strength of Co-PP and various FRPP tested at various temperatures.

better than that on the aminosilane-treated glass fiber (AGF). This superiority can be explained by that the functional group of epoxysilane may produce a stronger interface adhesive effect within the functional group of carboxylic acid of i-PP-*g*-AA. Therefore, stress is transmitted more

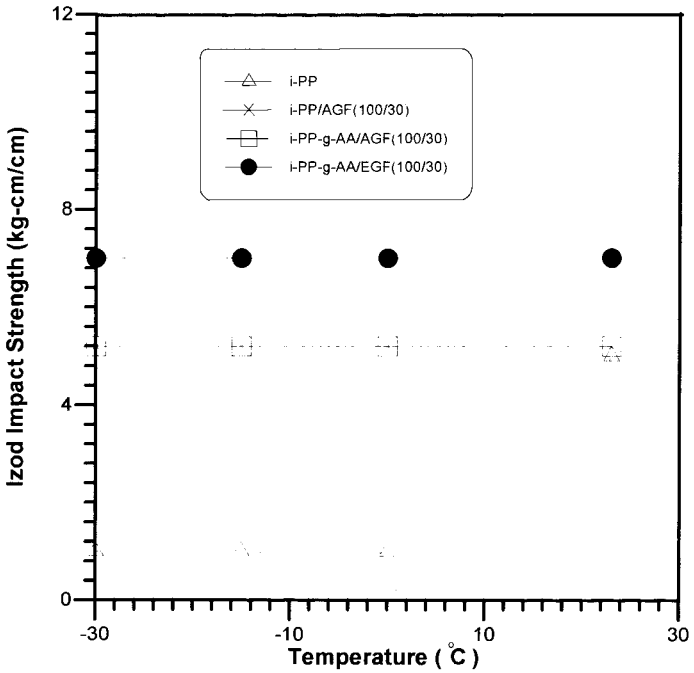

Figure 6 The notched Izod impact strength of i-PP and various FRPP tested at various temperatures.

Table I Mechanical Properties of PP and FRPP

Sample	Tensile Strength (kg/cm^2)	Flexural Strength (MPa)	Flexural Modulus (GPa)	HDT (°C)
Co-PP	238	19.4	1.9	113
Co-PP/AGF (100/30)	277	34.0	5.4	133
Co-PP-*g*-AA/AGF (100/30)	334	40.0	5.8	148
i-PP	320	33.7	3.1	119
i-PP/AGF (100/30)	350	43.0	5.7	138
i-PP-*g*-AA/AGF (100/30)	449	55.0	6.9	155
i-PP-*g*-AA/EGF (100/30)	561	66.0	7.5	159

Co-PP-*g*-AA = Co-PP grafted with AA; i-PP-*g*-AA = i-PP grafted with AA; AGF = glass fiber treated with aminosilane coupling agent; EGF = glass fiber treated with epoxysilane coupling agent.

efficiently, ultimately increasing the notched Izod impact strength. In summing up the results in Figures 5 and 6, we can conclude that Co-PP FRPP has a higher impact strength than has i-PP FRPP.

Stiffness and Heat-distortion Temperature (HDT)

Table I lists the variations in the tensile strength of glass fiber-reinforced Co-PP and i-PP. Initially, the tensile strength of i-PP/AGF is only slightly lower than that of i-PP. Nevertheless, the tensile strength of i-PP-*g*-AA/EGF significantly exceeds that of i-PP-*g*-AA/AGF. The above observation can analyzed as follows: The AA-grafting i-PP-*g*-AA, on its side chain, possesses the functional group —COOH which can easily form a chemical bond with the functional group $—NH_2$ of aminosilane to produce amides. Such a bonding effect can transmit the stress applied on the i-PP matrix to the reinforced glass fiber and, consequently, increase the blends' tensile strength. Comparing the tensile strengths of both i-PP-*g*-AA/AGF and i-PP-*g*-AA/EGF blends reveals that i-PP-*g*-AA/EGF has a higher tensile strength than that of i-PP-*g*-AA/AGF. This higher tensile strength can be attributed to a better bonding force between the functional groups —COOH and $—CH—CH_2$ (O) of epoxysilane and, hence, better stress transmission. Table I displays the variations of tensile strength of the Co-PP FRPP matrix. This table reveals a similar trend to that of the i-PP FRPP matrix. The Co-PP FRPP matrix possesses a generally lower tensile strength than that of the i-PP FRPP matrix, as attributed to the fact that the former has a lower tensile strength than that of the latter.

Both flexural strength and flexural modulus can be used to interpret a material's stiffness, that is, material with high magnitudes of both properties have a high stiffness. The fact that the mineral fillers generally used have a substantially higher stiffness than that of polymeric materials accounts for why the blending of mineral fillers undoubtedly increases the stiffness of polymeric materials. The ability to improve the wettability of a matrix would also enable the interface adhesion to be improved. Correspondingly, the quantity of mineral fillers and their reinforcing effect is increased. Table I summarizes the effect on the flexural strength and flexural modulus from this improved interface. According to this table, i-PP obviously increases in flexural strength and flexural modulus after AGF reinforcement. If i-PP further undergoes AA grafting, the interface adhesion between i-PP-*g*-AA and AGF can be further improved and the flexural strength and flexural modulus of i-PP-*g*-AA/AGF becomes higher than that of i-PP/AGF. The reason why i-PP-*g*-AA/EGF possesses the highest flexural strength and flexural modulus is that the epoxysilane functional group forms a better bond with i-PP-*g*-AA. While the changes in flexural strength and flexural modulus with the Co-PP FRPP matrix can also be understood in Table I, changes in the Co-PP FRPP system also resemble the i-PP FRPP matrix; however, the average values of Co-PP are lower than those of i-PP with the same filler content. This phenomenon may be attributed to the flexural strength and flexural modulus of Co-PP, which are not as good as those of i-PP.

Table I also presents the HDT of both Co-PP and i-PP matrixes. As with other mechanical properties, the HDT of both blends is closely re-

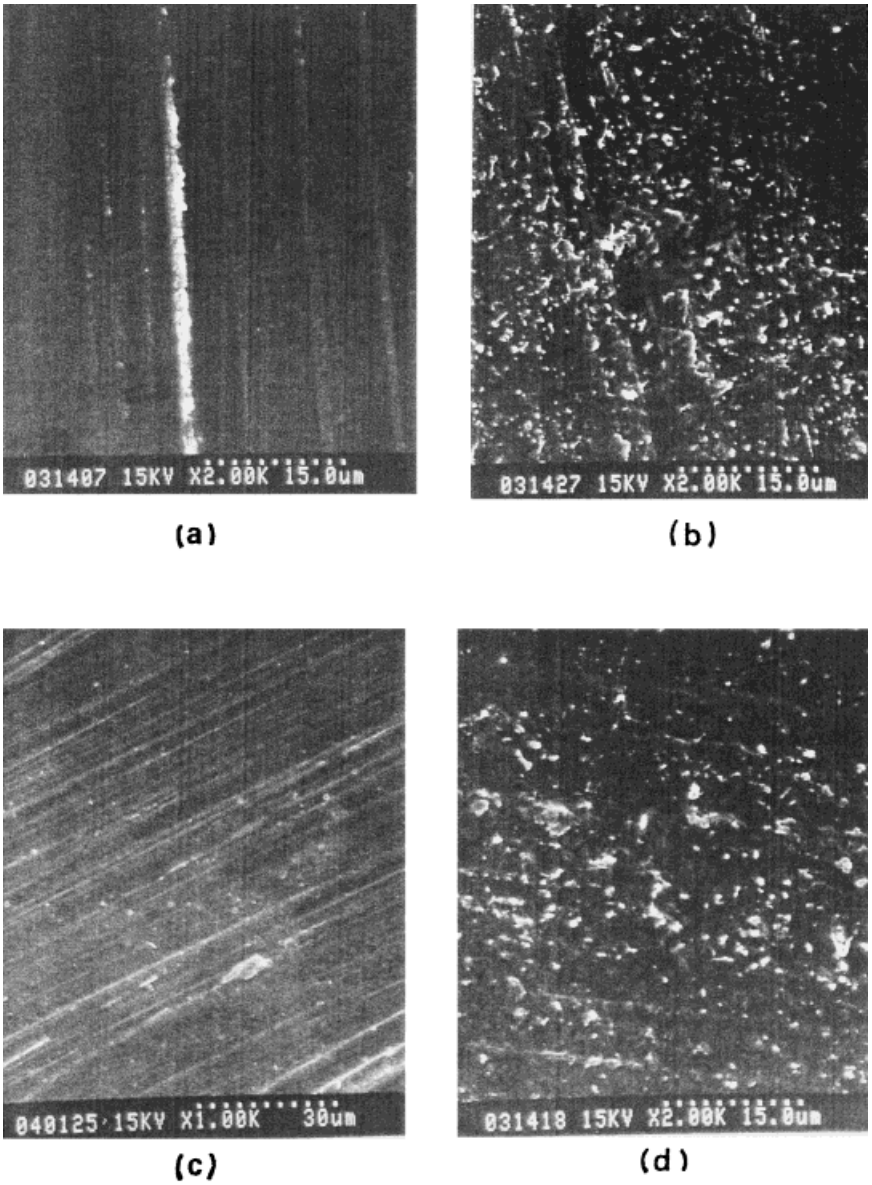

Figure 7 Scanning electron micrographs of (a) i-PP, (b) i-PP-*g*-AA (3 phr AA), (c) Co-PP, and (d) Co-PP-*g*-AA (3 phr AA) film.

lated to the interfacial adhesion. The better the interface adhesion implies a higher HDT. The fact that the HDT of i-PP exceeds Co-PP accounts for why the HDT of the i-PP blends is correspondingly higher than that of the Co-PP blends with the same filler content. Furthermore, according to Nielsen,[19] the behavior of the flexural modulus with the filler content is the same as that of HDT with the filler content. Restated, the HDT is increased due to the flexural modulus. In summing up the observations in Table I, we can conclude that the HDT and stiffness of the material are, to some extent, related.

Structure of Grafting Matrices and Their Composition

Morphology of Grafting Matrices and Their Composition

To observe the morphological change of PP prior to and after AA grafting, films were made with heat compression at 190°C. The films were made of Co-PP, i-PP, as well as Co-PP-*g*-AA and i-PP-*g*-AA with AA grafting in various ratios. The surface of these films was coated with gold for SEM observation.

Figure 7 compares the photos of (a) i-PP, (c)

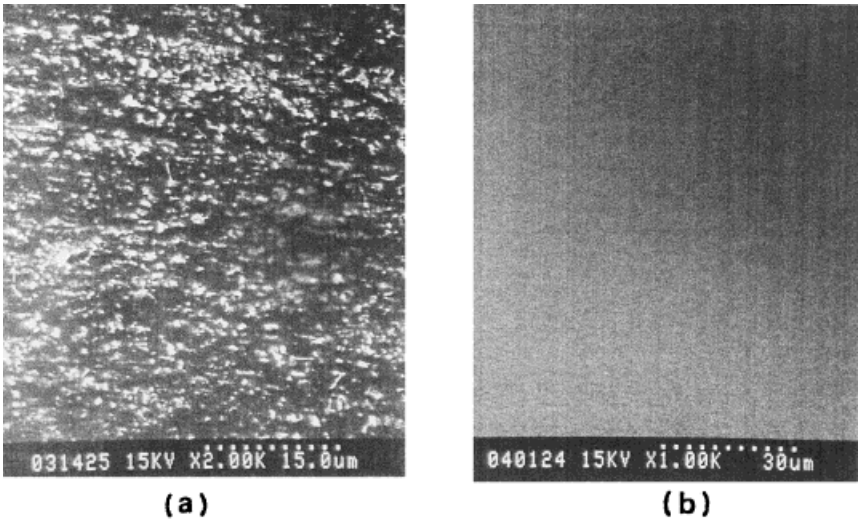

Figure 8 Scanning electron micrographs of (a) Co-PP-*g*-AA (7 phr AA), and (b) PAA film.

Co-PP, and (b) i-PP-*g*-AA and (d) Co-PP-*g*-AA with 3 phr AA grafting. Among them, in both i-PP-*g*-AA and Co-PP-*g*-AA, PAA was washed away by xylene. For both (b) i-PP-*g*-AA and (d) Co-PP-*g*-AA, all existing particle structures that also appeared in that of PP-*g*-AA and PE-*g*-AA underwent a photografting reaction.[20,21] The formation of particles is attributed to the aggregation of AA on the side chain since AA is hydrophilic and PP is hydrophobic. Moreover, Figure 8(a) presents an SEM photo for 7 phr AA grafting Co-PP-*g*-AA (PAA was washed away by xylene), which exhibits more particles of that structure. Figure 8(b) is an SEM photo of pure PAA that does not contain the particle structures found in Figure 8(a) because aggregation did not occur with pure PAA. The pure PAA was prepared in the following manner: A measure of the BPO initiator was initially dissolved in acetone while adding three measures of AA. The entire solution was then spread on Teflon film and allowed to polymerize at 60°C for 1 h. The above discussion, reveals that the particle structures in grafting PP are formed by hydrophilic

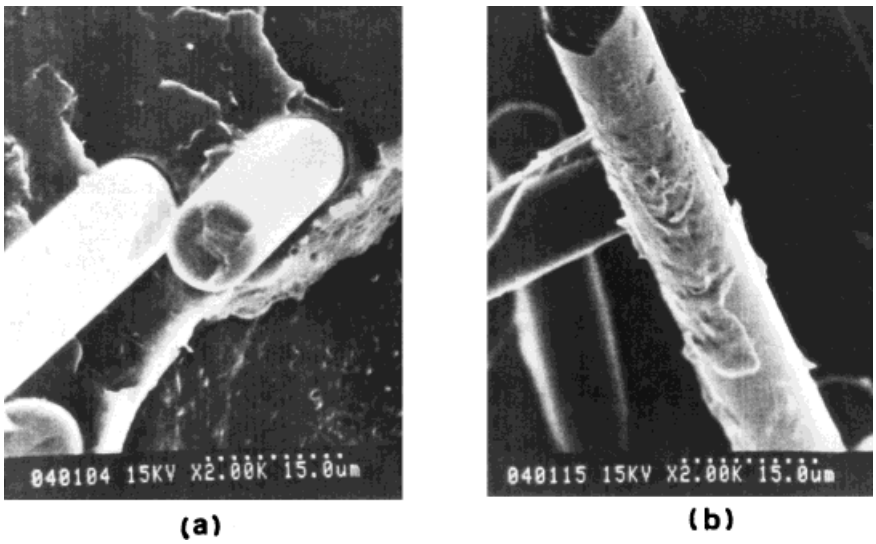

Figure 9 Scanning electron micrographs of impact fractured (at 25°C) surface of (a) Co-PP/AGF (100/30) and (b) Co-PP-*g*-AA (3 phr AA)/AGF (100/30).

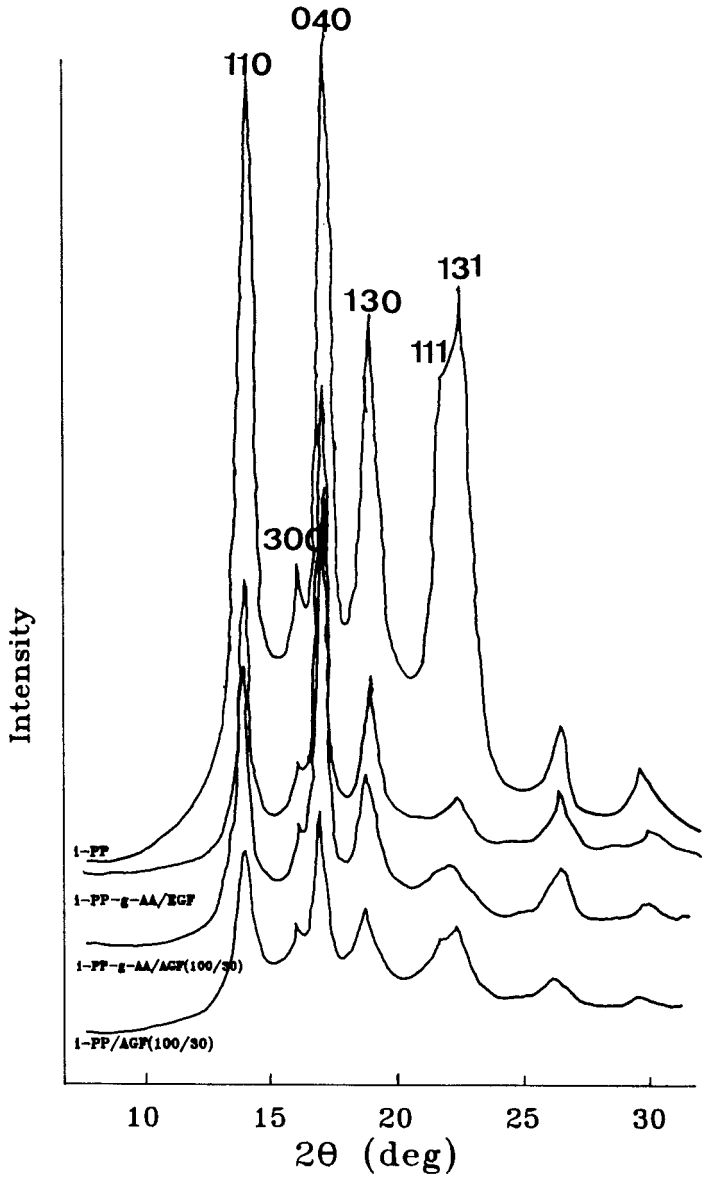

Figure 10 WAXS diffractograms of i-PP with various FRPP.

AA aggregates in hydrophobic PP. However, such particle structures are not formed in PAA because aggregation did not occur with PAA itself.

Interfacial Adhesion Between Grafting PP and FRPP

The reinforcing effect on all FRPP blends is ordered as follows: Co-PP-*g*-AA/AGF > Co-PP/AGF and i-PP-*g*-AA/EGF > i-PP-*g*-AA/AGF > i-PP/AGF; such results can be attributed to the various improvements obtained for interface adhesion between the glass fiber and matrices. To examine the adhesive improvements of FRPP interfaces, SEM was used to observe the FRPP fractured section from the impact test at room temperature. Figures 9(a,b) display the SEM photos of fractured sections of Co-PP/AGF and Co-PP-*g*-AA/AGF, respectively. Comparing the two photos reveals that there is an indication of no wettability on the smooth glass fiber surface in Figure 9(a). However, in Figure 9(b), a layer of Co-PP-*g*-AA is attached to the glass fiber surface, implying that interfacial adhesion is improved by grafted AA.

Effects of Grafting Matrices on Crystal Structure

Figure 10 presents WAXS analyses for i-PP and all FRPP, indicating the following: (1) The WAXS

Table II Crystalline Size of PP and FRPP

Sample	(110) Crystallite Size (D_{hkl}) (nm)	(040) Crystallite Size (D_{hkl}) (nm)
Co-PP	4.849	6.043
Co-PP/AGF (100/30)	4.735	5.674
Co-PP-*g*-AA/AGF (100/30)	4.717	5.518
i-PP	4.662	6.034
i-PP/AGF (100/30)	4.490	5.747
i-PP-*g*-AA/AGF (100/30)	4.329	4.827
i-PP-*g*-AA/EG (100/30)	4.041	5.486

$D_{hkl} = K\,\lambda/\beta \cos\theta$ (crystalline size, nm). $K = 0.9$ (proportionality factor). $\lambda = 1.5418$ nm (wavelength). β: width of half-height (radians). Co-PP-*g*-AA: Co-PP grafted with AA. i-PP-*g*-AA: i-PP grafted with AA. AGF: glass fiber treated with aminosilane coupling agent. EGF: glass fiber treated with epoxysilane coupling agent.

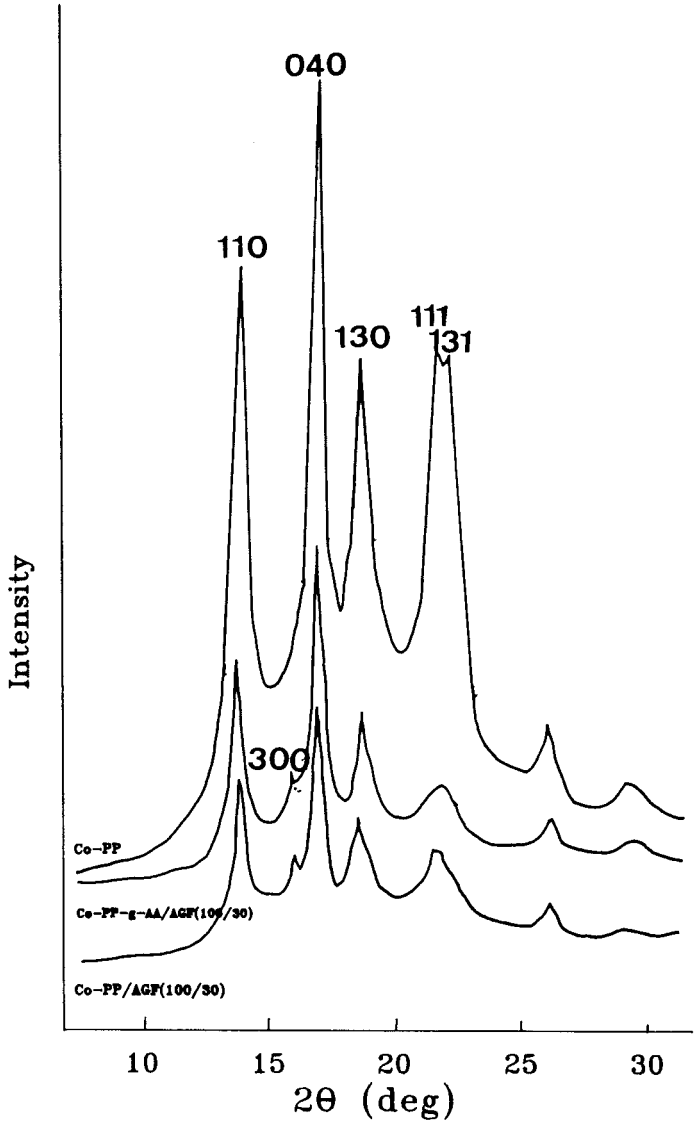

Figure 11 WAXS diffractograms of Co-PP with various FRPP.

curve characteristic peaks of FRPP correspond to those of i-PP; neither do they increase nor decrease. Neither blending of glass fiber nor i-PP grafting changes the original i-PP crystal type. (2) The drop of every characteristic peak suggests that spherulites have become smaller due to the blending of the glass fiber and the use of BPO in the grafting process. Table II reveals the crystalline size of PP and FRPP. Such a smaller crystallized structure can enhance the fixing for glass fiber and is beneficial to FRPP. Figure 11 presents the analyses of WAXS for Co-PP and all FRPP matrices. Figure 11 differs from Figure 10 in that after AGF is added a characteristic peak appears at $2\theta = 16$ of Co-PP, which did not originally exist. Such characteristic peaks are the spherulite lattice of the β-form (300). The blending of glass fiber not only introduces many different phase nuclei, but also activates the formation of β-form spherulites.[22–24]

CONCLUSIONS

This work grafted AA on the side chain of Co-PP and i-PP matrices using a twin-screw extruder in the melt-mixing method. Specimens were produced by injection molding. Based on the results presented herein, we can conclude the following:

1. The effects on the grafting ratio and grafting efficiency from AA-grafted i-PP are more significant than those from AA-grafted Co-PP. This discrepancy may be attributed to that i-PP has more 3^0H than has Co-PP. In addition, the AA-grafting efficiency decreases with increasing AA concentration.
2. The AA grafting to PP demonstrates excellent interface adhesion with the glass fiber. SEM analyses confirm that Co-PP, having undergone AA grafting, has an increased wettability on the glass fiber, thereby enhancing interfacial adhesion and ultimately upgrading the mechanical properties of FRPP (e.g., tensile strength, flexural strength, flexural modulus, and HDT). Moreover, the impact strength of grafted FRPP remains nearly unaffected at low temperatures.
3. With Co-PP-*g*-AA and i-PP-*g*-AA, all particle structures exist owing to that hydrophilic AA aggregates in the hydrophobic matrices. However, in this study, aggregation did not occur with PAA itself.
4. WAXS analysis indicates that a BPO initiator can refine PP crystals by a nucleation agent. Adding glass fiber decreases the crystals' size. Such a crystallized structure elevates the fixing for glass fiber and, therefore, is beneficial to FRPP.

REFERENCES

1. I. Sasaki and F. Ide, *Kobunshi Ronbunshu,* **38,** 67 (1981).
2. B. Ranby and F. Z. Guo, *Polym. Adv. Technol.,* **5,** 829 (1994).
3. W. Xiao, J. Yao, and X. Huang, *J. Func. Mater.,* **25,** 317 (1994).
4. I. Sasaki, T. Kodama, and F. Ide, *Kobunsh Ronbunshu,* **32,** 645 (1975).
5. I. Sasaki and F. Ide, *Kobunshi Ronbunshu.,* **38,** 75 (1981).
6. B. D. Favis, J. L. Blanchard, and R. E. Praudhmoe, *J. Appl. Polym. Sci.,* **28,** 1235 (1983).
7. M.-A. Romero and A. Donad, *Polymer,* **35,** 5342 (1994).
8. E. Papirer and V. T. Nguyen, *Polym. Lett.,* **10,** 167 (1972).
9. S. Yamashita and S. Kohjiya, *J. Appl. Polym. Sci.,* **17,** 2935 (1973).
10. L. J. Dogue, N. Mermilliod, and A. Fandini, *J. Appl. Polym. Sci.,* **56,** 33 (1995).
11. P. Bajaj, N. K. Jha, and R. K. Jha, *Polym. Eng. Sci.,* **29,** 557 (1989).
12. K. Hashilmoto, T. Fujusawa, M. Kobayashi, and R. Yosomiya, *J. Appl. Polym. Sci.,* **27,** 4529 (1982).
13. H. Yoshida and F. Higashide, *J. Appl. Polym. Sci.,* **18,** 939 (1974).
14. N. Ferg, R. Laible, and K. Hamann, *Angew. Makromol. Chem.,* **34,** 81 (1973).
15. T. E. Lipatova and I. S. Skorynina, *J. Polym. Sci.* C-16, 2341 (1967).
16. F. Runge, H. Ehrhardt, and G. Penndorf, *Makromol. Chem.,* **81,** 68 (1965).
17. W.-Y. Chiang and W.-D. Yang, *J. Appl. Polym. Sci.,* **35,** 807 (1988).
18. D. R. Moore and L. J. Mathias, *J. Appl. Polym. Sci.,* **32,** 6299 (1986).
19. L. E. Nielsen, *Mechanical Properties of Polymer and Composites,* Vol. 2, Marcel Dekker, New York, 1974, p. 341.
20. Y. Ogiwara and H. Kubota, *J. Polym. Sci. Polym. Lett. Ed.,* **23,** 365 (1985).
21. H. Kubota, N. Koike, Y. Ogiwara, and Y. Hata, *J. Polym. Sci. Part C Polym. Lett.,* **25,** 273 (1987).
22. R. T. Samules and R. Y. Tee, *J. Polym. Sci. A-2,* **10,** 385 (1972).
23. A. J. Lovinger, J. O. Chua, and C. C. Gryte, *J. Polym. Sci. Phys. Ed.,* **15,** 641 (1977).
24. J. L. Kardos, A. W. Christiansen, and E. Baer, *J. Polym. Sci. Phys. Ed.,* **4,** 777 (1966).